JACS
JOURNAL OF THE AMERICAN CHEMICAL SOCIETY
pubs.acs.org/JACS
Article

Molecular Ball Joints: Mechanochemical Perturbation of Bullvalene Hardy–Cope Rearrangements in Polymer Networks

Peiguan B. Sun, Meredith N. Pomfret, Matthew J. Elardo, Adhya Suresh, Ángel Rentería-Gómez, Remy F. Lalisse, Sheila Keating, Chuqiao Chen, Shayna L. Hilburg, Progyateg Chakma, Yunze Wu, Rowina C. Bell, Stuart J. Rowan, Osvaldo Gutierrez, and Matthew R. Golder*

Cite This: J. Am. Chem. Soc. 2024, 146, 19229–19238
Read Online
ACCESS | Metrics & More | Article Recommendations | Supporting Information

ABSTRACT: The solution-state fluxional behavior of bullvalene has fascinated physical organic and supramolecular chemists alike. Little effort, however, has been put into investigating bullvalene applications in bulk, partially due to difficulties in characterizing such dynamic systems. To address this knowledge gap, we herein probe whether bullvalene Hardy–Cope rearrangements can be mechanically perturbed in bulk polymer networks. We use dynamic mechanical analysis to demonstrate that the activation barrier to the glass transition process is significantly elevated for bullvalene-containing materials relative to "static" control networks. Furthermore, bullvalene rearrangements can be mechanically perturbed at low temperatures in the glassy region; such behavior facilitates energy dissipation (i.e., increased hysteresis energy) and polymer chain alignment to stiffen the material (i.e., increased Young's modulus) under load. Computational simulations corroborate our work that showcases bullvalene as a reversible "low-force" covalent mechanophore in the modulation of viscoelastic behavior.

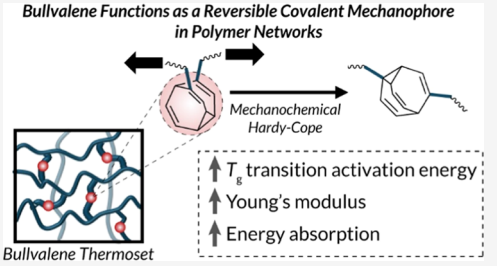

INTRODUCTION

Recent advances in polymer mechanochemistry have led to the development of force-responsive materials.[1,2] Incorporating force-responsive small molecules (e.g., mechanophores) into polymer networks introduces novel properties such as cargo release[3−5] or stress visualization.[6−8] Many related systems are prized, however, for their "sacrificial bonds" that can dissipate exogenous force and enhance mechanical properties. Materials with such bonds can generally be separated into two categories, noncovalent ("low-force" activation) (Figure 1A) and covalent ("high-force" activation) (Figure 1B), depending on how the mechanically active units are structured. Noncovalent systems take advantage of supramolecular interactions and/or mechanical bonds;[9−13] specific examples include soft materials containing folded proteins,[14] $\pi-\pi$ aromatic stacking,[15−18] hydrogen bonding,[19−25] metal–organic motifs,[26−31] rotaxanes,[32−34] and catenanes.[19,35−40] Adaptations in these systems are generally reversible with low activation barriers. On the other hand, systems bearing covalent mechanophores use higher energy barrier chemical transformations to adapt to applied mechanical force (e.g., pericyclic reaction). Specific examples include reversible retro-[4 + 2] Diels–Alder reactions for adaptable materials and nonreversible cycloreversions for tear resistance or toughening.[41−46] While there are no examples to date of low-force materials mediated by covalent bonds (i.e., chemical reactions), we envisioned the potential for "shapeshifting" molecular cages to provide access to this class of materials with a novel energy absorption motif (Figure 1C).

One of the most studied molecular shapeshifters, bullvalene, was first synthesized by Doering, Roth, and Schröder in the 1960s and since then has fascinated chemists due to its unique molecular architecture.[47,48] Three alkenes emanating from a central carbon atom, organized symmetrically in a boat conformation, and connected by a strained cyclopropane ring sets up ideal conditions for rapid Hardy–Cope rearrangements.[49] Unsubstituted bullvalene has more than 1.2 million (10!/3) degenerate isomers rapidly interconverting (E_a = ca. 11 kcal/mol) at room temperature (Figure 2A).[50,51]

Supramolecular interactions can perturb the interconversion of fluxional isomers for applications in molecular recognition (Figure 2B).[52−55] Such substituted bullvalenes, when unperturbed, exist in an equilibrium distribution of valence isomers. Upon addition of analytes, bullvalene engages in guest–host interactions, shifting to a new equilibrium population. Accessing such multisubstituted bullvalenes, however, is difficult due to lengthy synthetic sequences.[56,57] Recent progress in concisely accessing substituted bullvalenes

Received: March 29, 2024
Revised: June 25, 2024
Accepted: June 26, 2024
Published: July 4, 2024

https://doi.org/10.1021/jacs.4c04401
J. Am. Chem. Soc. 2024, 146, 19229–19238

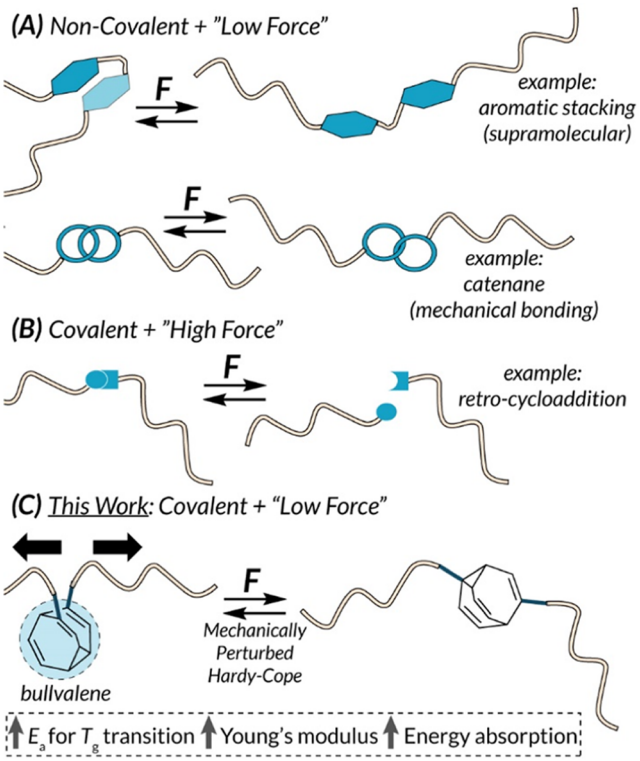

Figure 1. Overview of mechanically responsive soft materials making use of (A) low-force supramolecular interactions or mechanical bonds, (B) high-force covalent bonds, and (C) low-force shape-shifting covalent molecular cages (e.g., bullvalene).

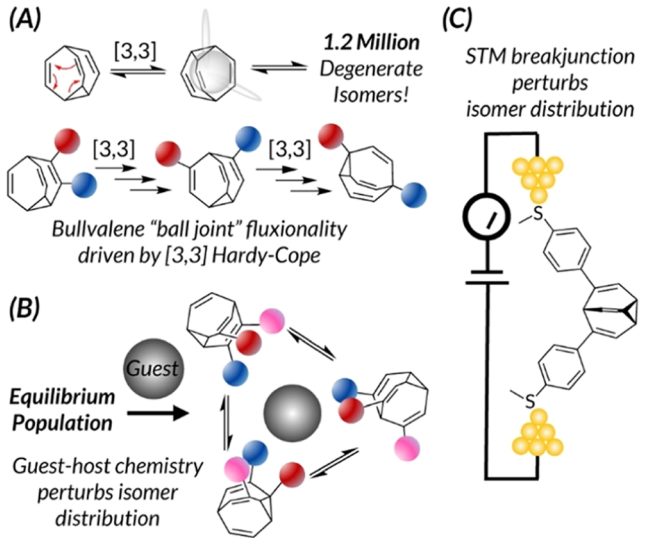

Figure 2. (A) Illustration of rapid bullvalene Hardy–Cope rearrangements. (B) Bullvalene adjusts equilibrium population upon guest–host interactions. (C) Bullvalene employed as a single-molecule circuit junction capable of adapting to the STMBJ movement.

reported by Fallon reignited interest in bullvalene applications.[58,59] Most applications of bullvalene explored so far are the solution state, however.

Interestingly, examples of bullvalene rearrangements in the solid state also exist.[60,61] Specifically, dynamic behaviors were observed in unsubstituted bullvalene single crystals with an activation barrier for Hardy–Cope rearrangements resembling those in isotropic and liquid crystalline solutions. More recently, Darwish and Fallon demonstrated the mechanical control of bullvalene fluxionality in a scanning tunneling microscopy breakjunction (STMBJ). Perturbed isomerization facilitates dynamic piezoresistance (Figure 2C).[62] Our previous work on incorporating bullvalene into π-rich thermoplastics showed that stochastic bullvalene isomers could effectively modulate the rigidity of such polymers but left many unanswered questions about resultant thermomechanical behaviors.[63]

Since bullvalene's valence isomer distribution can adapt to exogenous stimuli in solution and in the bulk (Figure 2),[52−54,60−62] we imagined that upon applied mechanical force within a bulk material, the equilibrium population of bullvalene could adapt to the applied force vector. We envisioned that studying the thermomechanical properties of these materials would be an ideal way to understand molecular-level sigmatropic rearrangements within polymer networks. If reversible Hardy–Cope rearrangements can be perturbed through mechanical force, we might expect unique thermoset properties by bridging the gap between "low force" and "covalently bonded" force-responsive materials in a strictly nonscissile system (Figure 1C). Herein, we incorporate bullvalene into elastomeric polymer networks to study their thermal behavior and temperature-dependent viscoelastic properties alongside control networks containing "static" cross-linkers. Using dynamic mechanical analysis (DMA), we demonstrate that bullvalene rearrangements not only increase the activation barrier for the glass transition process but also lead to distinct stiffening and energy dissipation behaviors below the glass transition temperature (i.e., glassy region). Furthermore, we computationally explore the impact of external force on discrete bullvalene isomers and identify two plausible "mechanophore" pathways that may contribute to the observed properties. These collective thermal and mechanical properties unique to bullvalene thermosets provide credence for the consequences of molecular fluxionality on bulk materials properties.

RESULTS AND DISCUSSION

Network Synthesis. The requisite cross-linked elastomers for thermal and mechanical testing were synthesized from *n*-butyl acrylate and an appropriate diacrylate cross-linker under thermal free radical conditions (V-70, 60 °C) that we have confirmed bullvalene tolerates (Figure S1). We selected cross-linker loadings between 2 and 7 mol % in the preparation for thermal and mechanical experiments (i.e., **X-Net-Y**). The cross-linker for target bullvalene networks (**Bull-Net-Y**), bullvalene diacrylate (**Bull-DA**), is derived from dimethanol bullvalene **5**, the product of Co-catalyzed formal [6 + 2] cycloaddition of silyl-protected 2-butyne-1,4-diol **2** and cyclooctatetraene (COT) after deprotection.[51,58,64] Photochemical di-π-methane rearrangement[65−67] to **4** and subsequent esterification with acrylic acid affords **Bull-DA** (Scheme 1A). In the selection of control static cross-linkers, we first chose adamantane diacrylate (**Ad-DA**). Bullvalene and adamantane are both C_{10} hydrocarbon cages with similar molar masses. Conveniently, substituents on adamantane are also situated in a nonplanar fashion, akin to bullvalene's geometry. As **Bull-DA** and **Ad-DA** should have similar steric profiles, we can probe the effect of cross-linker topology and fluxionality on bulk materials properties through the synthesis of **Ad-Net-Y**. These two **X-DA** cross-linkers were used to access homogeneous **X-Net-Y** materials (**Y** = 7, 5, and 2 mol %) as

https://doi.org/10.1021/jacs.4c04401
J. Am. Chem. Soc. 2024, 146, 19229−19238

Scheme 1. Synthesis of X-Net-Y Polymer Networks[a]

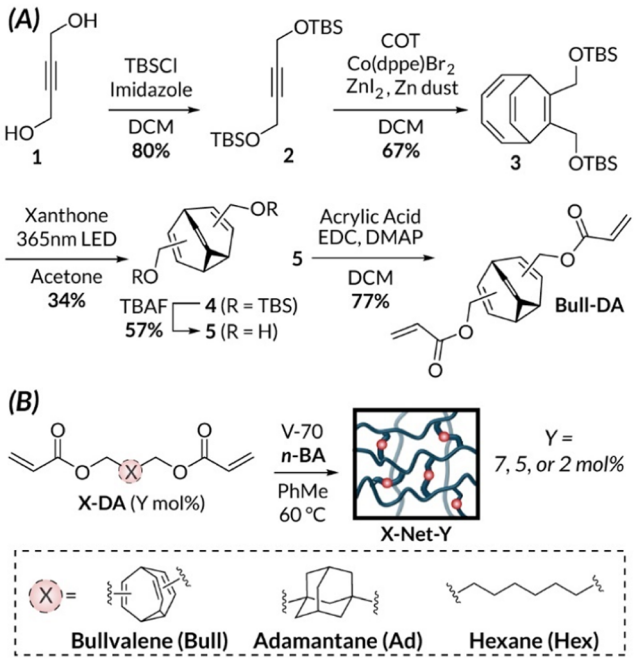

[a](A) Synthesis of **Bull-DA.** (B) Preparation of *n*-butyl acrylate thermosets (**X-Net-Y**).

well as "mixed" **Bull$_{2.5}$Ad$_{2.5}$-Net-5** and **Bull$_{1.25}$Ad$_{3.75}$-Net-5** materials to further interrogate the role of bullvalene within cross-linked materials. In addition, we controlled for cross-linker rigidity by utilizing commercially available 1,6-hexanediol diacrylate (**Hex-DA**) as a second control cross-linker toward **Hex-Net-Y** (Scheme 1B).

Comparison of Physical Properties. The physical properties of the resulting networks (ca. 80% monomer conversion; Table S1) **Bull-Net-7**, **Ad-Net-7**, and **Hex-Net-7** were characterized using a variety of analytical techniques. Thermal gravimetric analysis (TGA; Figure S2) confirms that all materials have similar decomposition temperatures (T_d = 364−377 °C), and helium pycnometry demonstrates that all materials have the same densities (ρ = 1.06−1.09 g/cm^3; Table S2) at 25 °C. To further interrogate network structure, we performed small-angle X-ray scattering (SAXS) on **Bull-Net-7** and **Ad-Net-7** (Figure S3). Both bulk samples exhibit relatively featureless SAXS curves indicative of no long-range order; a lack of sharp features indicates a lack of crystalline and/or highly ordered domains. Tensile plateau moduli (E'_0) measured using DMA frequency sweep experiments at 20 °C confirm that all materials have E'_0 (0.261, 0.269, 0.405 MPa for **Bull-Net-7**, **Ad-Net-7**, and **Hex-Net-7**, respectively) on the same order of magnitude (Figure S4). These data suggest that **Bull-Net-7** and **Ad-Net-7** have similar entanglement molecular weights, while **Hex-Net-7** has shorter distances between cross-links. The glass transition temperatures of these materials were also characterized through modulated differential scanning calorimetry (MDSC). Analysis of the total heat flow shows that **Bull-Net-7** and **Ad-Net-7** have similar $T_{g,DSC}$ (−34 and −37 °C, respectively) (Figure 3A), while **Hex-Net-7** has a lower $T_{g,DSC}$ (−42 °C), likely due to reduced cross-linker rigidity and/or increased cross-linker density.[68] For the less densely cross-linked materials (**X-Net-5** and **X-Net-2**), adamantane, bullvalene, and mixed networks' $T_{g,DSC}$ remained similar (Figures 3B,C and S5). We also performed swelling experiments in several organic solvents (methylene chloride, acetone, ethyl acetate, dimethylformamide) to compare cross-linking densities across all **X-Net-7** materials (Figure S6). While **Bull-Net-7** consistently has the highest equilibrium swelling ratios, they are generally within 10−15% of that of **Ad-Net-7**. Cross-linker fluxionality (i.e., flexibility) may play a role in facilitating increased swelling for **Bull-Net-7**. On the other hand, **Hex-Net-7** always has a much lower swelling ratio than **Bull-Net-7** in all solvents; we attribute these inconsistencies in swelling ratios potentially to differences in cross-linking steric and density. Due to the general similarities in monomer conversion, T_d, ρ, SAXS, $T_{g,DSC}$, E'_0, and swelling between **Bull-Net-7** and **Ad-Net-7**, we assume that network structures are comparable for the purposes of subsequent thermomechanical analyses. On the other hand, the comparative differences noted above for **Hex-Net-7** suggest that its network structure is not comparable and, therefore, serves as a negative control for subsequent studies.

Thermomechanical Analysis. With an enhanced understanding of **X-Net-Y** physical and thermal behaviors, we next turned to thermomechanical analysis. First, DMA temperature-sweep experiments were performed in the linear viscoelastic region under tension (1 Hz); thermomechanical $T_{g,DMA}$ of **Bull-Net-7**, **Ad-Net-7**, and **Hex-Net-7** were measured to be 4.6, −9.1, and −18 °C, respectively (Figure 4A), at the apex of each tan (δ) peak. **Bull-Net-7** has the broadest tan (δ) peak,

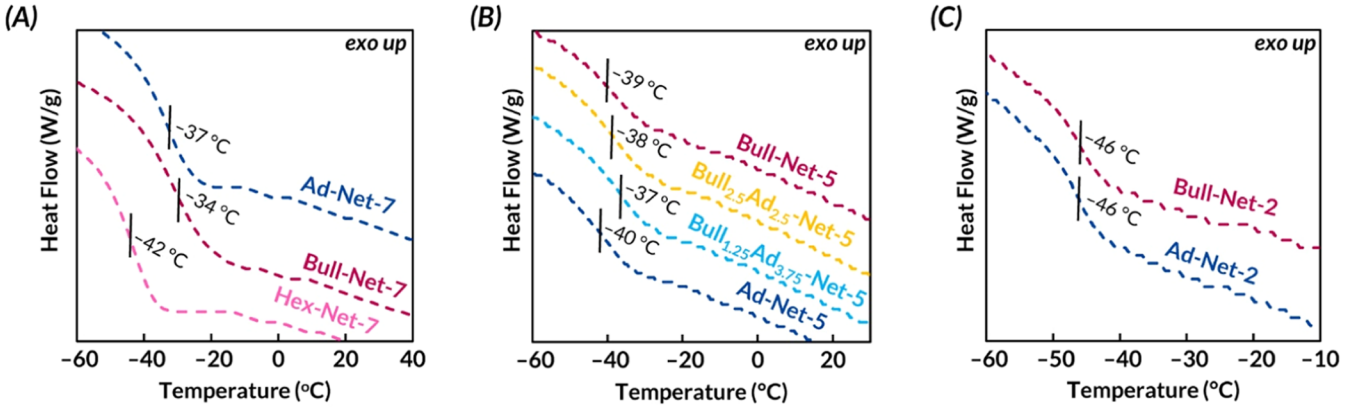

Figure 3. MDSC **X-Net-Y** total heat flow curves for (A) 7 mol % cross-linker loading (Y = 7), (B) 5 mol % cross-linker loading (Y = 5), including mixed materials derived from **Bull-DA** and **Ad-DA**, and (C) 2% cross-linker loading (Y = 2).

https://doi.org/10.1021/jacs.4c04401
J. Am. Chem. Soc. 2024, 146, 19229−19238

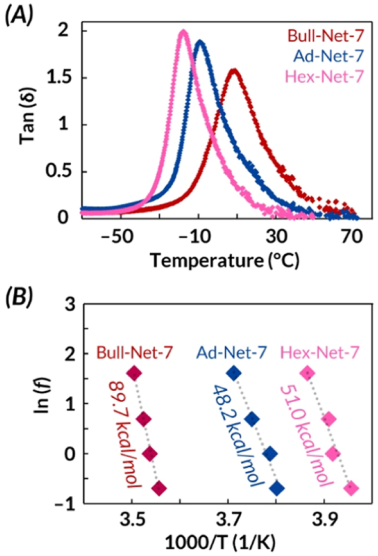

Figure 4. (A) Temperature-sweep experiments (1 Hz) of **X-Net-7** materials. (B) Arrhenius plots of $T_{g,DMA}$ of **X-Net-7** materials.

which suggests a more complex damping mechanism (*vide infra*) relative to **Ad-Net-7** and **Hex-Net-7**. It should be noted that while the span of $T_{g,DMA}$ values is larger than that for $T_{g,DSC}$, the onset of $T_{g,DMA}$ is quite similar across all materials. To quantify differences in these thermomechanical glass transition processes, the respective activation energies were calculated through multifrequency temperature-sweep experiments and fitting to the Arrhenius equation (Figures 4B and S7–S9).[69] Here, E_a for the **Bull-Net-7** $T_{g,DMA}$ transition (89.7 kcal/mol) is significantly higher than those for **Ad-Net-7** (48.2 kcal/mol) and **Hex-Net-7** (51.0 kcal/mol). This broader tan (δ) peak and elevated E_a for **Bull-Net-7** could be caused by an increase in fluxional rearrangements as the material approaches the glass transition temperature. As we describe in more detail below (see the Computational Mechanistic Investigations section), at lower temperatures under tension, the Hardy–Cope fluxionality may exist as a combination of mechanically guided thermal rearrangements (i.e., slowly interconverting bullvalenes "align" to the force vector) and/or mechanically activated rearrangements (i.e., discrete bullvalene isomers function as force-driven mechanophores).[70] These are not exhaustive options but rather serve as two plausible pathways that are conceptually related to STMBJ-driven bullvalene isomerization reported by Darwish and Fallon.[62]

In the case of a broader tan (δ) peak, the exact rearrangement pathway traversed by a particular bullvalene cross-linker likely varies across the continuum of the material due to local network inhomogeneities and/or cooperativity from neighboring bullvalene moieties. In other words, **Bull-Net-7** exhibits a wide range of molecular motion stemming from an ensemble of bullvalene rearrangements; the corresponding $T_{g,DMA}$ transition, therefore, occurs over a broader range of temperatures compared to **Ad-Net-7** and **Hex-Net-7**. In the case of **Bull-Net-7**'s elevated E_a for the $T_{g,DMA}$ transition, long-range segmental motion is restricted below $T_{g,DMA}$ and bullvalene has access to only a few immediate isomers that do not cause structural changes to the polymer network. As the temperature continues to increase while approaching $T_{g,DMA}$, molecular mobility dramatically increases. Consequently, there are more degrees of freedom for bullvalene to access additional isomers while adapting to the external force vector through a series of Hardy–Cope rearrangements. In doing so, energy is dissipated within the bullvalene cage (i.e., additional energy is required for sigmatropic rearrangements) and the observed E_a for **Bull-Net-7** is elevated relative to those of the control networks.

Importantly, despite **Ad-Net-7** acting as a "similar" network and **Hex-Net-7** acting as a "dissimilar" network relative to **Bull-Net-7**, **Bull-Net-7** retains the broadest tan (δ) peak and highest E_a for $T_{g,DMA}$ transition across all three materials. In fact, these trends hold true for bullvalene-containing **X-Net-5** materials as well (Table 1 and Figures S10–S16), suggesting

Table 1. Summary of X-Net-Y Temperature-Sweep Experiments

sample	$T_{g,DMA}$ (°C)[a]	E_a of T_g transition (kcal/mol)[b]
Bull-Net-7	4.6	89
Ad-Net-7	−9.1	48
Hex-Net-7	−18	51
Bull-Net-5	−11	56
$Bull_{2.5}Ad_{2.5}$-Net-5	−14	59
$Bull_{1.25}Ad3_{.75}$-Net-5	−15	44
Ad-Net-5	−13	34
Bull-Net-2	−25	41
Ad-Net-2	−28	39

[a]Reported from the apex of tan (δ) peak (1 Hz). [b]Calculated from an Arrhenius fit of multifrequency (5, 2, 1, 0.5 Hz) temperature-sweep experiments.

that cross-linker identity rather than network structure is a key driver in these phenomena. At lower cross-linker loadings (i.e., **Bull-Net-2** and **Ad-Net-2**), the minimal difference is observed in temperature-sweep experiments as longer distances between cross-links dilute the impacts of bullvalene described above.

Ad-Net-7 and **Bull-Net-7** were then subjected to frequency sweep experiments using DMA. In these experiments, we studied thermomechanical behavior across a range of temperatures and frequencies (1–100 Hz). We then generated master curves for each of the two networks spanning many decades of frequency using the principle of time–temperature superposition (Figures 5, S17, and S18). Master curves were generated by using appropriate shift factors with $T_{ref} = T_{g,DMA} - 20$ °C. While the master curves are generally comparable between **Ad-Net-7** and **Bull-Net-7**, further supporting our claim that these two thermosets have similar network structures, there is an interesting difference that is worth pointing out. The onset of the glassy region is more gradual near the edge of the glass transition region (higher frequency/lower temperature) in the case of **Bull-Net-7** compared to **Ad-Net-7**. In other words, E' and E'' level off more rapidly than what is observed for **Bull-Net-7** (Figure 5A). As a result, the corresponding tan (δ) curve (Figure 5B) for **Bull-Net-7** is broader than that for **Ad-Net-7**, akin to what was observed in our temperature-sweep experiments (Figure 4). In addition, this broadening observed in the **Bull-Net-7** tan (δ) curve is unsymmetrical; the curve tails significantly into the higher-frequency/lower-temperature region because of the more gradual onset of the glassy region as reflected in E' and E'' values. At higher temperatures well above $T_{g,DMA}$, it is known that bullvalene remains fluxional. When bullvalene is dynamic, we surmise that it can rapidly sample an ensemble of valence isomers and molecular motion is rapid. The rapid bullvalene

https://doi.org/10.1021/jacs.4c04401
J. Am. Chem. Soc. 2024, 146, 19229–19238

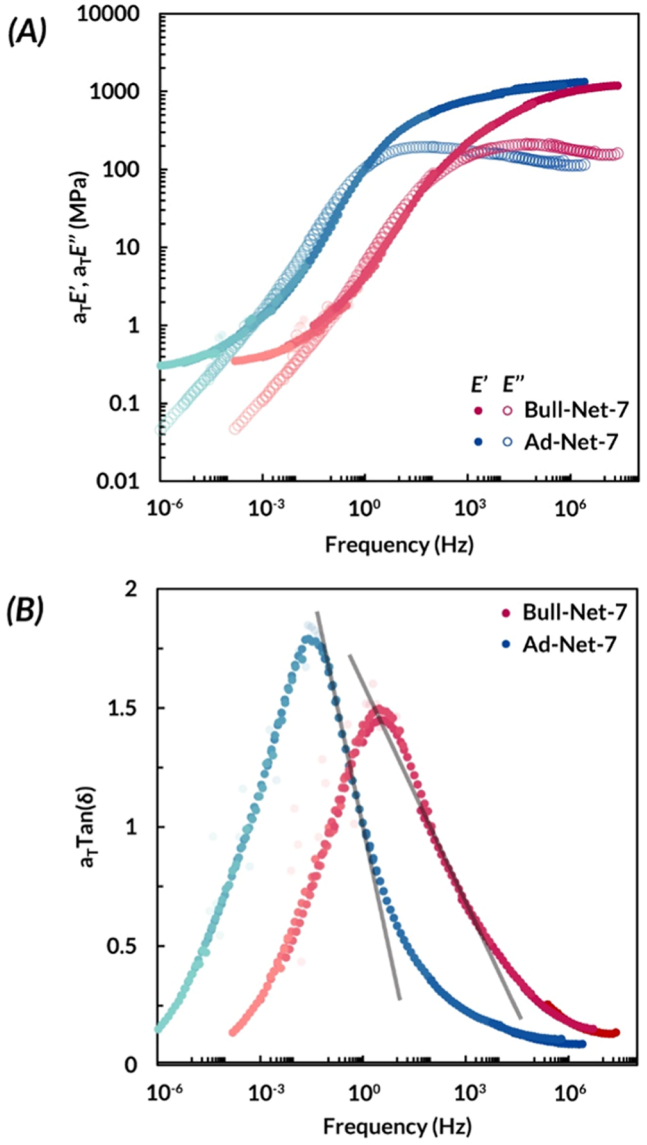

Figure 5. Master curves for **Ad-Net-7** and **Bull-Net-7** detailing (A) storage (E') and loss (E'') moduli and (B) tan (δ) (gray lines indicate differences in the high-frequency region).

fluxionality alongside freedom in molecular and chain mobility renders **Bull-Net-7** similar to **Ad-Net-7** at lower frequency/higher temperature. Our previous work studying bullvalene thermoplastics supports operative Hardy–Cope rearrangements throughout the polymer backbone as evidenced by enhanced thermal stability relative to unsaturated analogues.[63] As the temperature decreases and approaches $T_{g,DMA}$, macromolecular motion is limited and the bullvalene rearrangements slow down; some bullvalenes may even be kinetically trapped as static valence isomers. As energy is applied through oscillatory tension in frequency sweep experiments, bullvalene may rearrange to applied mechanical force (*vide infra*) by absorbing energy and guiding these rearrangements along the way. As a result, we hypothesize that the broadening of the **Bull-Net-7** tan (δ) curve and asymmetry at higher frequencies/lower temperatures is the consequence of less thermally active bullvalenes. The result is an ensemble of damping pathways, potentially involving disparate mechanically guided and/or mechanically activated Hardy–Cope rearrangements across a broad range of temperatures.

Tensile Experiments. To glean insight into potential temperature-dependent phenomena in **Bull-Net-X**, solution-state variable temperature NMR (VT-NMR) experiments (Figure 6A) were conducted on **Bull-DA**, which reveal slow chemical exchange at 25 °C consistent with E_a = ca. 11 kcal/mol; broad bullvalene vinyl proton (B_V), alkyl proton (B_A), and methylene linker proton (B_L) resonances around 5.9, 2.3, and 4.5 ppm, respectively, support this claim. When **Bull-DA** is cooled to −40 °C, B_V, B_A, and B_L resonances sharpen as the rate of chemical exchange via thermal Hardy–Cope rearrangements decreases further and approaches a static structure. Meanwhile, proton resonances not directly connected to the bullvalene cage (A, A', A'') actually broaden as bond rotation (E_a < 3 kcal/mol) slows on the NMR time scale. The differing dynamics between the chemical (i.e., bullvalene Hardy–Cope rearrangements) and physical (i.e., bond rotations) allow us to tame bullvalene fluxionality at lower temperatures, rendering bullvalene nearly static and confining it to a smaller quantity of valence isomers. In fact, these observations align well with the unique low-temperature behavior observed in **Bull-Net-Y** compared to **Ad-Net-Y** (*vide supra*). Thus, in order to probe mechanochemical perturbation and/or activation of Hardy–Cope rearrangements in bulk materials outside the linear viscoelastic region under tension, we reasoned that experiments needed to be conducted at lower temperatures where thermal bullvalene fluxionality becomes suppressed.

Examination of **X-Net-7** bulk energy dissipation behavior was carried out using DMA via cyclic loading experiments. At 20 °C, **Bull-Net-7**, as well as control network **Ad-Net-7**, display minimal hysteresis (Figures S19–S22). **Bull-Net-7** and **Ad-Net-7** also have similar Young's moduli (E = ca. 0.0022 MPa; Table S3). When the same cyclic loading experiments were carried out at −40 °C (Figures 6B and S23–S28), all materials displayed strain–stress curves known for a glassy polymer with little immediate recovery upon unloading.[71,72] While **Ad-Net-7** has noticeable energy dissipation characteristics (E_H = 2110 J/m^2), **Bull-Net-7** has nearly 3 times the hysteresis energy of **Ad-Net-7** (E_H = 6240 J/m^2) with enhanced stiffening (E = 8.5 MPa; Table S4).

It should be noted that the mechanism of deformation in materials below glass transition is different from conventional viscoelastic behavior above T_g. Instead of long-range disentanglement through chain sliding, bond cleavage and local molecular motion generally dominate.[68,71,72] Repeated cyclic loading of all **X-Net-7** materials at −40 °C does not show a loss in mechanical performance, thus confirming that minimal covalent bond cleavage occurs at a low temperature in **X-Net-7** materials.

To confirm that this behavior (Figure 6) is not due to variations in material density below $T_{g,DMA}$, we also performed thermal expansion experiments between 20 and −40 °C (Figure S29). As no significant differences were observed between **Bull-Net-7** and **Ad-Net-7**, corroboration with the pycnometry data (Table S2) implies comparatively low temperature densities. The observed differences in hysteresis energies may be attributed to differences in the relative stiffness and yield stress of these materials. For example, **Bull-Net-7** has a much higher Young's modulus (E = 8.5 MPa) relative to **Ad-Net-7** (E = 3.8 MPa). We hypothesize that unlike the sterically demanding adamantane, similarly sized bullvalene rearranges upon applied mechanical force (i.e.,

https://doi.org/10.1021/jacs.4c04401
J. Am. Chem. Soc. 2024, 146, 19229–19238

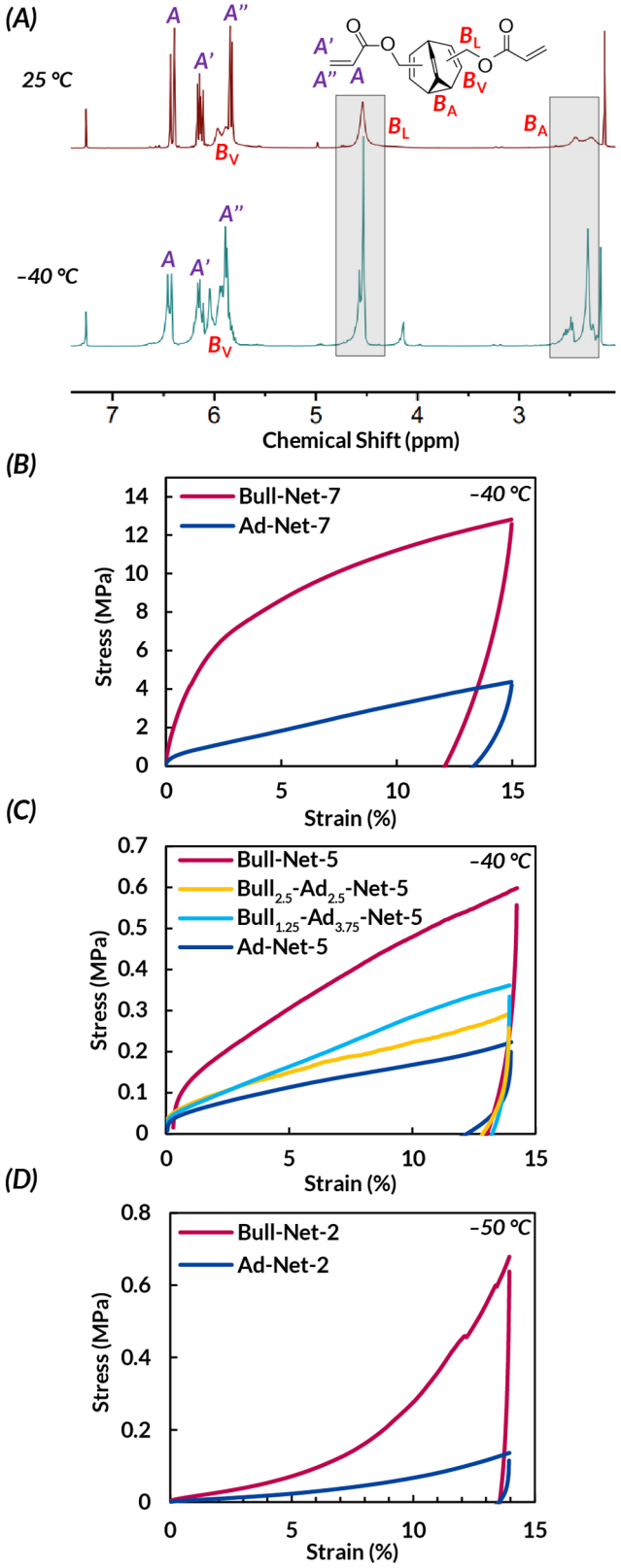

Figure 6. (A) VT ^{1}H NMR spectrum of **Bull-DA**. Cyclic loading of **X-Net-Y** materials: (B) Y = 7, (C) Y = 5, and (D) Y = 2.

"molecular ball joint") to further realign the already packed polymer strands together and make the material stiffer (Figure 7). In other words, as the rate of bullvalene Hardy–Cope rearrangements decreases at a lower experimental temperature,

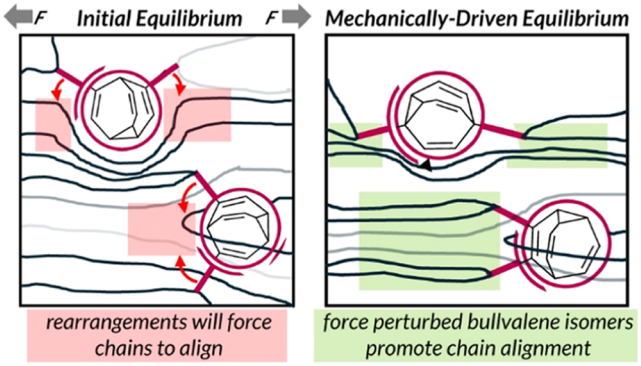

Figure 7. (A) Bullvalene adapts to applied force (B) through chain alignment governed by mechanically guided and/or mechanically activated Hardy–Cope rearrangements.

there is an opportunity to guide the valence isomer trajectory and/or activate certain isomers with external mechanical force. Additionally, without free segmental motion, the initial input mechanical energy can be first "absorbed" in **Bull-Net-7** by bullvalene rearrangements and the subsequent realignment of polymer chains. The result is that **Bull-Net-7** has a much higher yield stress (ca. 6 MPa at ca. 2% strain) compared to **Ad-Net-7** (yield stress <1 MPa at <1% strain) in the shear yielding process.[71,72] In other words, at low temperatures, **Bull-Net-7** has increased stiffness and yield stress relative to control networks; these properties contribute to the high hysteresis energy for **Bull-Net-7** driven by the sigmatropic rearrangement. These phenomena are not limited to **X-Net-7**; analogous **Ad-Net-Y** and **Bull-Net-Y** with a lower cross-linker loading (Y = 2 or 5 mol %) show similar trends in tensile properties (Figure 6C,D and Table 2). We also tested the same mixed

Table 2. Summary of X-Net-Y Tensile Results

sample	Young's modulus, E (MPa)	hysteresis energy, E_H (kJ/m^2)
Bull-Net-7[a]	8.50	6.24
Ad-Net-7[a]	3.80	2.11
Hex-Net-7[a]	0.110	0.805
Bull-Net-5[a]	1.00	0.226
$Bull_{2.5}Ad_{2.5}$-Net-5[a]	0.640	0.198
$Bull_{1.25}Ad_{3.75}$-Net-5[a]	0.680	0.141
Ad-Net-5[a]	0.600	0.0979
Bull-Net-2[b]	0.810	0.124
Ad-Net-2[b]	0.029	0.0301

[a]Data collected at −40 °C. [b]Data collected at −50 °C.

systems previously used to study $T_{g,DMA}$ (Table 1) and found that **$Bull_{2.5}Ad_{2.5}$-Net-5** and **$Bull_{1.25}Ad3_{.75}$-Net-5** have intermediary E and E_H relative to **Bull-Net-5** and **Ad-Net-5**; these data further support our claim that bullvalene incorporation enhances mechanical properties. Furthermore, these processes were all demonstrated to be fully reversible; when **X-Net-7** materials are allowed to warm to room temperature between successive loading at −40 °C, minimal changes in the resulting stress–strain curves are observed (Figures S30–S32).

Computational Mechanistic Investigations. To explain the unique material behaviors described above, we probed how an external mechanical force impacts bullvalene stability and associated Hardy–Cope rearrangement pathways. To do so, we turned to constrained geometries simulate external force

https://doi.org/10.1021/jacs.4c04401
J. Am. Chem. Soc. 2024, 146, 19229–19238

(CoGEF) simulations (see the Supporting Information for details).[73−75] We note that these calculations do not consider competitive thermal Hardy−Cope rearrangements and rather only consider the impact of exogenous force on individual static bullvalene valence isomers. To initiate our investigations, we first minimized derivatives of the 12 possible geometric isomers of **Bull-DA** (i.e., dimethylbullvalene analogues **B1**−**B12**; Figure S33) and calculated the energy profiles for thermal Hardy−Cope interconversions (Figures S35−S41) using unrestricted DFT at the B3LYP-D3/def2svp CPCM(DCM) level of theory. Next, for each bullvalene isomer, we simulated the impact of applying an external force on these isomers to "pull" them apart by increasing the relative distance between the two alkyl substituents (increments of 0.05 Å over 50 steps) on the bullvalene core until a C−C bond homolysis or a mechanochemical event occurred (Figures S41−S43). For isomers **B1**−**B4** and **B6**−**B10**, biradical formation occurs via the methyl group homolytic bond extrusion or bullvalene backbone scission (Figures S41−S43 and Table S5).[75] However, these processes are prohibitively high in energy (>75 kcal/mol between the ground state geometry of each isomer prior to biradical formation) and interestingly do not involve the formation of a radical on the potentially capricious cyclopropane ring in bullvalene. Taken together, based on the reversibility observed in cyclic loading−unloading experiments on **Bull-Net-7** (Figures S30−S32) and these calculations, this high-force (>ca. 4 nN) deleterious mechanochemical bullvalene decomposition is unlikely under our experimental conditions. On the other hand, increasing the distance between substituents in isomers **B11** and **B12** drives the Hardy−Cope rearrangement via the collapse to another isomer (i.e., **B11** → **B4** and **B12** → **B3**). Notably, these events are much lower energy processes (ca. 20−35 kcal/mol) and can proceed with lower calculated forces (<ca. 4 nN) (Figure S43 and Table S5). Thus, in addition to potentially "guiding" the trajectory of thermal Hardy−Cope rearrangements ($\Delta E^{\ddagger}$ < ca. 15 kcal/mol; Figures S34−S40) under mechanical tension, we also present another plausible mechanism that treats two discrete bullvalene valence isomers as mechanophores capable of undergoing mechanically activated Hardy−Cope rearrangements. While it is difficult to probe specific valence isomer interconversions within each **Bull-Net-Y** material, one potential force-responsive pathway could involve two mechanochemical Hardy−Cope rearrangements (large geometrical changes, **B12** → **B3** and **B11** → **B4**) joined by mechanically guided thermal Hardy−Cope rearrangement (minimal geometrical change, **B3** → **B11**) (Figure 8).

CONCLUSIONS

In summary, we report the utility of low-barrier Hardy−Cope rearrangements under strain in polymer networks by incorporating fluxional bullvalenes into *n*-butyl acrylate-based thermoset elastomers. DMA temperature-sweep experiments quantitatively demonstrate that bullvalene can dissipate energy more effectively than static controls, thereby increasing the activation energy for the glass transition process. While thermomechanical testing supports similar behavior between bullvalene (**Bull-Net-Y**) and adamantane (**Ad-Net-Y**) cross-linked materials at room temperature, frequency sweep experiments suggest that rearrangements can be activated mechanochemically as the rate of bullvalene Hardy−Cope rearrangements decrease at a lower temperature. Cyclic loading experiments at temperatures below $T_{g,DMA}$ demonstrate that

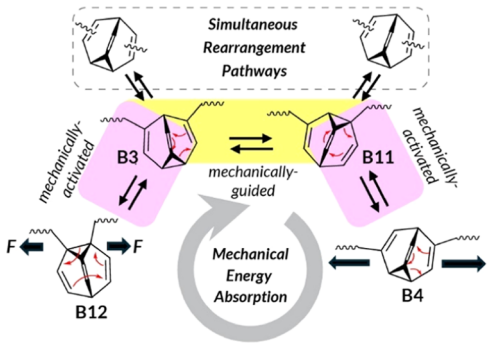

Figure 8. Representative proposed mechanism of action where mechanically activated (pink) and mechanically guided (yellow) Hardy−Cope rearrangements facilitate mechanical energy absorption in **Bull-Net-Y** materials.

Bull-Net-Y is much stiffer with a high hysteresis energy. Comparisons with **Ad-Net-7** suggest that bullvalene's ability to rearrange upon applied mechanical force facilitates chain alignment and stiffens the material upon loading. Finally, CoGEF simulations are employed to demonstrate the stability of the bullvalene cage under an external mechanical force while also revealing two "mechanically competent" valence isomers capable of engaging in mechanically activated Hardy−Cope rearrangements. Overall, having a simple unimolecular "ball joint" moiety that can dissipate energy through reversible sigmatropic rearrangements shows great potential for enhancing the durability of existing thermosets and opens new opportunities for impact- and vibration-resistant materials.

ASSOCIATED CONTENT

Supporting Information

The Supporting Information is available free of charge at https://pubs.acs.org/doi/10.1021/jacs.4c04401.

Experimental and synthetic procedures, solution-state and bulk characterization data, and thermal and mechanical testing data (PDF)

AUTHOR INFORMATION

Corresponding Author

Matthew R. Golder − *Department of Chemistry and Molecular Engineering & Science Institute, University of Washington, Seattle, Washington 98115, United States;* orcid.org/0000-0001-5848-7366; Email: goldermr@uw.edu

Authors

Peiguan B. Sun − *Department of Chemistry and Molecular Engineering & Science Institute, University of Washington, Seattle, Washington 98115, United States;* orcid.org/0000-0003-3036-4465

Meredith N. Pomfret − *Department of Chemistry and Molecular Engineering & Science Institute, University of Washington, Seattle, Washington 98115, United States;* orcid.org/0009-0001-7584-043X

Matthew J. Elardo − *Department of Chemistry and Molecular Engineering & Science Institute, University of Washington, Seattle, Washington 98115, United States;* orcid.org/0009-0007-6217-0338

Adhya Suresh − *Department of Chemistry, Texas A&M University, College Station, Texas 77843, United States*

https://doi.org/10.1021/jacs.4c04401
J. Am. Chem. Soc. 2024, 146, 19229−19238

Ángel Rentería-Gómez − *Department of Chemistry, Texas A&M University, College Station, Texas 77843, United States*
Remy F. Lalisse − *Department of Chemistry, Texas A&M University, College Station, Texas 77843, United States;* orcid.org/0000-0002-4556-5641
Sheila Keating − *Department of Chemistry, University of Chicago, Chicago, Illinois 60637, United States;* orcid.org/0000-0002-8189-1073
Chuqiao Chen − *Pritzker School of Molecular Engineering, University of Chicago, Chicago, Illinois 60637, United States;* orcid.org/0000-0002-4844-5098
Shayna L. Hilburg − *Department of Chemical Engineering, University of Washington, Seattle, Washington 98115, United States;* orcid.org/0000-0003-0825-7698
Progyateg Chakma − *Department of Chemistry and Molecular Engineering & Science Institute, University of Washington, Seattle, Washington 98115, United States*
Yunze Wu − *Department of Chemistry and Molecular Engineering & Science Institute, University of Washington, Seattle, Washington 98115, United States*
Rowina C. Bell − *Department of Chemistry and Molecular Engineering & Science Institute, University of Washington, Seattle, Washington 98115, United States*
Stuart J. Rowan − *Department of Chemistry, University of Chicago, Chicago, Illinois 60637, United States; Pritzker School of Molecular Engineering, University of Chicago, Chicago, Illinois 60637, United States; Argonne National Laboratory, Argonne, Illinois 60439, United States;* orcid.org/0000-0001-8176-0594
Osvaldo Gutierrez − *Department of Chemistry, Texas A&M University, College Station, Texas 77843, United States;* orcid.org/0000-0001-8151-7519

Complete contact information is available at: https://pubs.acs.org/10.1021/jacs.4c04401

Funding

This material is based upon the work supported by the U.S. Army Research Office (W911NF-23-1-0106 to M.R.G.), the donors of the American Chemical Society Petroleum Research Fund (62163-DNI7 to M.R.G.), generous start-up funds from the University of Washington, and NIH NIGMS (R35GM137797 to O.G.) for funding. M.J.E. acknowledges the National Science Foundation Graduate Research Fellowship Program (DGE-2140004) for a graduate research fellowship. DSC and DMA instrumentation were made possible through funding from the Student Technology Fund (STF) at the University of Washington. NMR spectroscopy resources at the University of Washington are supported by NIH (S10 OD030224-01A1). The authors also acknowledge the use of facilities and instrumentation (SAXS) supported by the U.S. National Science Foundation through the Major Research Instrumentation (MRI) program (DMR-2116265) and the UW Molecular Engineering Materials Center (MEM-C), a Materials Research Science and Engineering Center (DMR-2308979).

Notes

The authors declare no competing financial interest.

■ ACKNOWLEDGMENTS

The authors thank Prof. Dianne Xiao for the use of a TGA instrument. Dr. Martin Sadilek and Brandon Bol are acknowledged for assistance with mass spectrometry and DMA instrumentation. Prof. Aniruddh Vashisth, Prof. Alshakim Nelson, Prof. Lilo D. Pozzo, and Dr. Naroa Sadaba are acknowledged for their helpful discussions. The authors also acknowledge the Texas A&M University HPRC resources for providing computational resources (https://hprc.tamu.edu).

■ REFERENCES

(1) Willis-Fox, N.; Rognin, E.; Aljohani, T. A.; Daly, R. Polymer Mechanochemistry: Manufacturing Is Now a Force to Be Reckoned With. *Chem* **2018**, *4* (11), 2499−2537.
(2) Ghanem, M. A.; Basu, A.; Behrou, R.; Boechler, N.; Boydston, A. J.; Craig, S. L.; Lin, Y.; Lynde, B. E.; Nelson, A.; Shen, H.; Storti, D. W. The Role of Polymer Mechanochemistry in Responsive Materials and Additive Manufacturing. *Nat. Rev. Mater.* **2021**, *6* (1), 84−98.
(3) Küng, R.; Göstl, R.; Schmidt, B. M. Release of Molecular Cargo from Polymer Systems by Mechanochemistry. *Chem. - Eur. J.* **2022**, *28* (17), No. e202103860.
(4) Larsen, M. B.; Boydston, A. J. Flex-Activated" Mechanophores: Using Polymer Mechanochemistry To Direct Bond Bending Activation. *J. Am. Chem. Soc.* **2013**, *135* (22), 8189−8192.
(5) Zeng, T.; Ordner, L. A.; Liu, P.; Robb, M. J. Multimechanophore Polymers for Mechanically Triggered Small Molecule Release with Ultrahigh Payload Capacity. *J. Am. Chem. Soc.* **2024**, *146* (1), 95−100.
(6) Davis, D. A.; Hamilton, A.; Yang, J.; Cremar, L. D.; Van Gough, D.; Potisek, S. L.; Ong, M. T.; Braun, P. V.; Martínez, T. J.; White, S. R.; Moore, J. S.; Sottos, N. R. Force-Induced Activation of Covalent Bonds in Mechanoresponsive Polymeric Materials. *Nature* **2009**, *459* (7243), 68−72.
(7) Ducrot, E.; Chen, Y.; Bulters, M.; Sijbesma, R. P.; Creton, C. Toughening Elastomers with Sacrificial Bonds and Watching Them Break. *Science* **2014**, *344* (6180), 186−189.
(8) Sagara, Y.; Traeger, H.; Li, J.; Okado, Y.; Schrettl, S.; Tamaoki, N.; Weder, C. Mechanically Responsive Luminescent Polymers Based on Supramolecular Cyclophane Mechanophores. *J. Am. Chem. Soc.* **2021**, *143* (14), 5519−5525.
(9) Sivakova, S.; Rowan, S. J. Nucleobases as Supramolecular Motifs. *Chem. Soc. Rev.* **2005**, *34* (1), 9−21.
(10) Voorhaar, L.; Hoogenboom, R. Supramolecular Polymer Networks: Hydrogels and Bulk Materials. *Chem. Soc. Rev.* **2016**, *45* (14), 4013−4031.
(11) Xia, D.; Wang, P.; Ji, X.; Khashab, N. M.; Sessler, J. L.; Huang, F. Functional Supramolecular Polymeric Networks: The Marriage of Covalent Polymers and Macrocycle-Based Host−Guest Interactions. *Chem. Rev.* **2020**, *120* (13), 6070−6123.
(12) Zhu, Y.; Zheng, W.; Wang, W.; Yang, H.-B. When Polymerization Meets Coordination-Driven Self-Assembly: Metallo-Supramolecular Polymers Based on Supramolecular Coordination Complexes. *Chem. Soc. Rev.* **2021**, *50* (13), 7395−7417.
(13) Zheng, B.; Wang, F.; Dong, S.; Huang, F. Supramolecular Polymers Constructed by Crown Ether-Based Molecular Recognition. *Chem. Soc. Rev.* **2012**, *41* (5), 1621−1636.
(14) Smith, P. T.; Narupai, B.; Tsui, J. H.; Millik, S. C.; Shafranek, R. T.; Kim, D.-H.; Nelson, A. Additive Manufacturing of Bovine Serum Albumin-Based Hydrogels and Bioplastics. *Biomacromolecules* **2020**, *21* (2), 484−492.
(15) Miller, K. A.; Dodo, O. J.; Devkota, G. P.; Kirinda, V. C.; Bradford, K. G. E.; Sparks, J. L.; Hartley, C. S.; Konkolewicz, D. Aromatic Foldamers as Molecular Springs in Network Polymers. *Chem. Commun.* **2022**, *58* (37), 5590−5593.
(16) Traeger, H.; Sagara, Y.; Berrocal, J. A.; Schrettl, S.; Weder, C. Strain-Correlated Mechanochromism in Different Polyurethanes Featuring a Supramolecular Mechanophore. *Polym. Chem.* **2022**, *13* (19), 2860−2869.
(17) Burattini, S.; Greenland, B. W.; Merino, D. H.; Weng, W.; Seppala, J.; Colquhoun, H. M.; Hayes, W.; Mackay, M. E.; Hamley, I. W.; Rowan, S. J. A Healable Supramolecular Polymer Blend Based on

Aromatic Π−π Stacking and Hydrogen-Bonding Interactions. *J. Am. Chem. Soc.* **2010**, *132* (34), 12051−12058.
(18) Wang, F.; Liao, R.; Wang, F. Pathway Control of π-Conjugated Supramolecular Polymers by Incorporating Donor-Acceptor Functionality. *Angew. Chem., Int. Ed.* **2023**, *62* (36), No. e202305827.
(19) Chen, L.; You, W.; Wang, J.; Yang, X.; Xiao, D.; Zhu, H.; Zhang, Y.; Li, G.; Yu, W.; Sessler, J. L.; Huang, F. Enhancing the Toughness and Strength of Polymers Using Mechanically Interlocked Hydrogen Bonds. *J. Am. Chem. Soc.* **2024**, *146* (1), 1109−1121.
(20) Song, Y.; Liu, Y.; Qi, T.; Li, G. L. Towards Dynamic but Supertough Healable Polymers through Biomimetic Hierarchical Hydrogen-Bonding Interactions. *Angew. Chem., Int. Ed.* **2018**, *57* (42), 13838−13842.
(21) Xing, P.; Li, Y.; Xue, S.; Fiona Phua, S. Z.; Ding, C.; Chen, H.; Zhao, Y. Occurrence of Chiral Nanostructures Induced by Multiple Hydrogen Bonds. *J. Am. Chem. Soc.* **2019**, *141* (25), 9946−9954.
(22) Zhang, Q.; Li, T.; Duan, A.; Dong, S.; Zhao, W.; Stang, P. J. Formation of a Supramolecular Polymeric Adhesive via Water−Participant Hydrogen Bond Formation. *J. Am. Chem. Soc.* **2019**, *141* (20), 8058−8063.
(23) Scherman, O. A.; Ligthart, G. B. W. L.; Ohkawa, H.; Sijbesma, R. P.; Meijer, E. W. Olefin Metathesis and Quadruple Hydrogen Bonding: A Powerful Combination in Multistep Supramolecular Synthesis. *Proc. Natl. Acad. Sci. U.S.A.* **2006**, *103* (32), 11850−11855.
(24) Cordier, P.; Tournilhac, F.; Soulié-Ziakovic, C.; Leibler, L. Self-Healing and Thermoreversible Rubber from Supramolecular Assembly. *Nature* **2008**, *451* (7181), 977−980.
(25) Sijbesma, R. P.; Beijer, F. H.; Brunsveld, L.; Folmer, B. J. B.; Hirschberg, J. H. K. K.; Lange, R. F. M.; Lowe, J. K. L.; Meijer, E. W. Reversible Polymers Formed from Self-Complementary Monomers Using Quadruple Hydrogen Bonding. *Science* **1997**, *278* (5343), 1601−1604.
(26) Diao, K.; J Whitaker, D.; Huang, Z.; Qian, H.; Ren, D.; Zhang, L.; Li, Z.-Y.; Sun, X.-Q.; Xiao, T.; Wang, L. An Ultralow-Acceptor-Content Supramolecular Light-Harvesting System for White-Light Emission. *Chem. Commun.* **2022**, *58* (14), 2343−2346.
(27) Zhukhovitskiy, A. V.; Zhong, M.; Keeler, E. G.; Michaelis, V. K.; Sun, J. E. P.; Hore, M. J. A.; Pochan, D. J.; Griffin, R. G.; Willard, A. P.; Johnson, J. A. Highly Branched and Loop-Rich Gels via Formation of Metal−Organic Cages Linked by Polymers. *Nat. Chem.* **2016**, *8* (1), 33−41.
(28) McConnell, A. J.; Wood, C. S.; Neelakandan, P. P.; Nitschke, J. R. Stimuli-Responsive Metal−Ligand Assemblies. *Chem. Rev.* **2015**, *115* (15), 7729−7793.
(29) Yount, W. C.; Loveless, D. M.; Craig, S. L. Small-Molecule Dynamics and Mechanisms Underlying the Macroscopic Mechanical Properties of Coordinatively Cross-Linked Polymer Networks. *J. Am. Chem. Soc.* **2005**, *127* (41), 14488−14496.
(30) Beck, J. B.; Rowan, S. J. Multistimuli, Multiresponsive Metallo-Supramolecular Polymers. *J. Am. Chem. Soc.* **2003**, *125* (46), 13922−13923.
(31) Hailes, R. L. N.; Oliver, A. M.; Gwyther, J.; Whittell, G. R.; Manners, I. Polyferrocenylsilanes: Synthesis, Properties, and Applications. *Chem. Soc. Rev.* **2016**, *45* (19), 5358−5407.
(32) Okumura, Y.; Ito, K. The Polyrotaxane Gel: A Topological Gel by Figure-of-Eight Cross-Links. *Adv. Mater.* **2001**, *13* (7), 485−487.
(33) Jiang, L.; Liu, C.; Mayumi, K.; Kato, K.; Yokoyama, H.; Ito, K. Highly Stretchable and Instantly Recoverable Slide-Ring Gels Consisting of Enzymatically Synthesized Polyrotaxane with Low Host Coverage. *Chem. Mater.* **2018**, *30* (15), 5013−5019.
(34) Noda, Y.; Hayashi, Y.; Ito, K. From Topological Gels to Slide-Ring Materials. *J. Appl. Polym. Sci.* **2014**, *131* (15), No. 40509.
(35) Liu, C.; Morimoto, N.; Jiang, L.; Kawahara, S.; Noritomi, T.; Yokoyama, H.; Mayumi, K.; Ito, K. Tough Hydrogels with Rapid Self-Reinforcement. *Science* **2021**, *372* (6546), 1078−1081.
(36) Ito, K. Novel Cross-Linking Concept of Polymer Network: Synthesis, Structure, and Properties of Slide-Ring Gels with Freely Movable Junctions. *Polym. J.* **2007**, *39* (6), 489−499.
(37) Zhao, J.; Zhang, Z.; Cheng, L.; Bai, R.; Zhao, D.; Wang, Y.; Yu, W.; Yan, X. Mechanically Interlocked Vitrimers. *J. Am. Chem. Soc.* **2022**, *144* (2), 872−882.
(38) Hart, L. F.; Lenart, W. R.; Hertzog, J. E.; Oh, J.; Turner, W. R.; Dennis, J. M.; Rowan, S. J. Doubly Threaded Slide-Ring Polycatenane Networks. *J. Am. Chem. Soc.* **2023**, *145* (22), 12315−12323.
(39) Yang, X.; Cheng, L.; Zhang, Z.; Zhao, J.; Bai, R.; Guo, Z.; Yu, W.; Yan, X. Amplification of Integrated Microscopic Motions of High-Density [2]Rotaxanes in Mechanically Interlocked Networks. *Nat. Commun.* **2022**, *13* (1), No. 6654.
(40) Nosiglia, M. A.; Colley, N. D.; Danielson, M. K.; Palmquist, M. S.; Delawder, A. O.; Tran, S. L.; Harlan, G. H.; Barnes, J. C. Metalation/Demetalation as a Postgelation Strategy To Tune the Mechanical Properties of Catenane-Crosslinked Gels. *J. Am. Chem. Soc.* **2022**, *144* (22), 9990−9996.
(41) Chen, X.; Dam, M. A.; Ono, K.; Mal, A.; Shen, H.; Nutt, S. R.; Sheran, K.; Wudl, F. A Thermally Re-Mendable Cross-Linked Polymeric Material. *Science* **2002**, *295* (5560), 1698−1702.
(42) Stevenson, R.; De Bo, G. Controlling Reactivity by Geometry in Retro-Diels−Alder Reactions under Tension. *J. Am. Chem. Soc.* **2017**, *139* (46), 16768−16771.
(43) Bailey, S. J.; Barney, C. W.; Sinha, N. J.; Pangali, S. V.; Hawker, C. J.; Helgeson, M. E.; Valentine, M. T.; Read De Alaniz, J. Rational Mechanochemical Design of Diels−Alder Crosslinked Biocompatible Hydrogels with Enhanced Properties. *Mater. Horiz.* **2022**, *9* (7), 1947−1953.
(44) Wang, S.; Beech, H. K.; Bowser, B. H.; Kouznetsova, T. B.; Olsen, B. D.; Rubinstein, M.; Craig, S. L. Mechanism Dictates Mechanics: A Molecular Substituent Effect in the Macroscopic Fracture of a Covalent Polymer Network. *J. Am. Chem. Soc.* **2021**, *143* (10), 3714−3718.
(45) Wang, Z.; Zheng, X.; Ouchi, T.; Kouznetsova, T. B.; Beech, H. K.; Av-Ron, S.; Matsuda, T.; Bowser, B. H.; Wang, S.; Johnson, J. A.; Kalow, J. A.; Olsen, B. D.; Gong, J. P.; Rubinstein, M.; Craig, S. L. Toughening Hydrogels through Force-Triggered Chemical Reactions That Lengthen Polymer Strands. *Science* **2021**, *374* (6564), 193−196.
(46) Wang, S.; Hu, Y.; Kouznetsova, T. B.; Sapir, L.; Chen, D.; Herzog-Arbeitman, A.; Johnson, J. A.; Rubinstein, M.; Craig, S. L. Facile Mechanochemical Cycloreversion of Polymer Cross-Linkers Enhances Tear Resistance. *Science* **2023**, *380* (6651), 1248−1252.
(47) Doering, W. V.; Roth, W. R. A Rapidly Reversible Degenerate Cope Rearrangement: Bicyclo[5.1.0]Octa-2,5-Diene. *Tetrahedron* **1963**, *19* (5), 715−737.
(48) Schröder, G. Preparation and Properties of Tricyclo-[3,3,2,04,6]Deca-2,7,9-Triene (Bullvalene). *Angew. Chem., Int. Ed.* **1963**, *2* (8), 481−482.
(49) Cope, A. C.; Hardy, E. M. The Introduction of Substituted Vinyl Groups. V. A Rearrangement Involving the Migration of an Allyl Group in a Three-Carbon System1. *J. Am. Chem. Soc.* **1940**, *62* (2), 441−444.
(50) Bismillah, A. N.; Chapin, B. M.; Hussein, B. A.; McGonigal, P. R. Shapeshifting Molecules: The Story so Far and the Shape of Things to Come. *Chem. Sci.* **2020**, *11* (2), 324−332.
(51) Ferrer, S.; Echavarren, A. M. Synthesis of Bullvalenes: Classical Approaches and Recent Developments. *Synthesis* **2019**, *51* (5), 1037−1048.
(52) Birvé, A. P.; Patel, H. D.; Price, J. R.; Bloch, W. M.; Fallon, T. Guest-Dependent Isomer Convergence of a Permanently Fluxional Coordination Cage. *Angew. Chem., Int. Ed.* **2022**, *61* (9), No. e202115468.
(53) Bismillah, A. N.; Sturala, J.; Chapin, B. M.; Yufit, D. S.; Hodgkinson, P.; McGonigal, P. R. Shape-Selective Crystallisation of Fluxional Carbon Cages. *Chem. Sci.* **2018**, *9* (46), 8631−8636.
(54) Dohmen, C.; Paululat, T.; Ihmels, H. Reversible Restrain and Release of the Dynamic Valence Isomerization in a Shape-Shifting Bullvalene by Complex Formation. *Chem. - Eur. J.* **2024**, *30*, No. e202304311.

https://doi.org/10.1021/jacs.4c04401
J. Am. Chem. Soc. 2024, 146, 19229−19238

(55) Schröder, G.; Witt, W. Crown Ethers with Fluctuating Ring Size ("Breathing Crown Ethers"). *Angew. Chem., Int. Ed.* **1979**, *18* (4), 311−312.
(56) Teichert, J. F.; Mazunin, D.; Bode, J. W. Chemical Sensing of Polyols with Shapeshifting Boronic Acids As a Self-Contained Sensor Array. *J. Am. Chem. Soc.* **2013**, *135* (30), 11314−11321.
(57) Ferrer, S.; Echavarren, A. M. Synthesis of Barbaralones and Bullvalenes Made Easy by Gold Catalysis. *Angew. Chem., Int. Ed.* **2016**, *55* (37), 11178−11182.
(58) Yahiaoui, O.; Pašteka, L. F.; Judeel, B.; Fallon, T. Synthesis and Analysis of Substituted Bullvalenes. *Angew. Chem., Int. Ed.* **2018**, *57* (10), 2570−2574.
(59) Patel, H. D.; Tran, T.-H.; Sumby, C. J.; Pašteka, L. F.; Fallon, T. Boronate Ester Bullvalenes. *J. Am. Chem. Soc.* **2020**, *142* (8), 3680−3685.
(60) Müller, A.; Haeberlen, U.; Zimmermann, H.; Poupko, R.; Luz, Z. The Pathways of the Combined Cope Rearrangement—Molecular Reorientation Process in Solid Bullvalene: A Deuterium 2D Exchange NMR Study on a Single Crystal. *Mol. Phys.* **1994**, *81* (5), 1239−1258.
(61) Meier, B. H.; Earl, W. L. Fluxional Behavior in the Solid State: Bullvalene. *J. Am. Chem. Soc.* **1985**, *107* (19), 5553−5555.
(62) Reimers, J. R.; Li, T.; Birvé, A. P.; Yang, L.; Aragonès, A. C.; Fallon, T.; Kosov, D. S.; Darwish, N. Controlling Piezoresistance in Single Molecules through the Isomerisation of Bullvalenes. *Nat. Commun.* **2023**, *14* (1), No. 6089.
(63) Pomfret, M. N.; Sun, P. B.; Huang, Z.; Freund, A. C.; Miyoshi, T.; Golder, M. R. Stochastic Bullvalene Architecture Modulates Structural Rigidity in π-Rich Macromolecules. *Angew. Chem., Int. Ed.* **2023**, *62* (19), No. e202301695.
(64) Achard, M.; Mosrin, M.; Tenaglia, A.; Buono, G. Cobalt(I)-Catalyzed [6 + 2] Cycloadditions of Cyclooctatetra(Tri)Ene with Alkynes. *J. Org. Chem.* **2006**, *71* (7), 2907−2910.
(65) Zimmerman, H. E.; Mariano, P. S. Mechanistic and Exploratory Organic Photochemistry. XLI. Di-.Pi.-Methane Rearrangement. Interaction of Electronically Excited Vinyl Chromophores. *J. Am. Chem. Soc.* **1969**, *91* (7), 1718−1727.
(66) Zimmerman, H. E.; Grunewald, G. L. The Chemistry of Barrelene. III. A Unique Photoisomerization to Semibullvalene. *J. Am. Chem. Soc.* **1966**, *88* (1), 183−184.
(67) Zimmerman, H. E.; Binkley, R. W.; Givens, R. S.; Sherwin, M. A. Mechanistic Organic Photochemistry. XXIV. The Mechanism of the Conversion of Barrelene to Semibullvalene. A General Photochemical Process. *J. Am. Chem. Soc.* **1967**, *89* (15), 3932−3933.
(68) Hiemenz, P. C.; Lodge, T. *Polymer Chemistry*, 2nd ed.; CRC Press: Boca Raton, 2007.
(69) Li, G.; Lee-Sullivan, P.; Thring, R. W. Determination of Activation Energy for Glass Transition of an Epoxy Adhesive Using Dynamic Mechanical Analysis. *J. Therm. Anal. Calorim.* **2000**, *60* (2), 377−390.
(70) Izak-Nau, E.; Campagna, D.; Baumann, C.; Göstl, R. Polymer Mechanochemistry-Enabled Pericyclic Reactions. *Polym. Chem.* **2020**, *11* (13), 2274−2299.
(71) *The Physics of Glassy Polymers*, 2nd ed.; Haward, R. N.; Haward, R. N., Eds.; Chapman & Hall: London, 1997.
(72) Kausch, H. H.; Hassell, J. A.; Jaffee, R. I. Deformation and Fracture of High Polymers. *Science* **1973**, *181* (4103), 961−962.
(73) Beyer, M. K. The Mechanical Strength of a Covalent Bond Calculated by Density Functional Theory. *J. Chem. Phys.* **2000**, *112* (17), 7307−7312.
(74) Klein, I. M.; Husic, C. C.; Kovács, D. P.; Choquette, N. J.; Robb, M. J. Validation of the CoGEF Method as a Predictive Tool for Polymer Mechanochemistry. *J. Am. Chem. Soc.* **2020**, *142* (38), 16364−16381.
(75) Wick, C. R.; Topraksal, E.; Smith, D. M.; Smith, A.-S. Evaluating the Predictive Character of the Method of Constrained Geometries Simulate External Force with Density Functional Theory. *Forces Mech.* **2022**, *9*, No. 100143.

https://doi.org/10.1021/jacs.4c04401
J. Am. Chem. Soc. 2024, 146, 19229−19238